Coal Mining Deformation Monitoring Using SBAS-InSAR and Offset Tracking: A Case Study of Yu County, China

Yu Chen, Yunxiao Tong, and Kun Tan, *Senior Member, IEEE*

***Abstract*—Ground deformation caused by underground coal mining has a large subsidence gradient and high nonlinearity and may cause continuous destruction to the surface structure after mining. A synthetic aperture radar interferometry (InSAR) is a powerful method for measuring and reconstructing the ground displacement. In this article, a total of 19 descending orbit *X*-band TerraSAR-X and 16 ascending orbit *C*-band Sentinel-1 images were integrated to monitor the ground displacement of a coal mining area in Yu County (Hebei Province, China) using a small baseline subset (SBAS-InSAR) algorithm. We found that the SBAS-InSAR technology can obtain reliable results in regions without a high gradient deformation by combining the deformation rates derived from both the TerraSAR-X and Sentinel-1 datasets. The maximum subsidence rate was approximately 125 mm/y between 17 June 2015 and 07 January 2016. In the case of large-gradient deformation, it is indeed difficult to obtain the mining-induced surface subsidence information accurately using the conventional multitemporal (MT-InSAR) techniques owing to the limitations of the SAR wavelength. In response to this problem, a new decision-making fusion method based on SBAS-InSAR and offset tracking was developed to monitor the large-gradient settlement in mining areas. The results show that the method developed compensates for the shortcomings of the traditional MT-InSAR technologies in the field of large-gradient deformation and obtains reliable results.**

***Index Terms*—Coal mining, decision-making fusion, ground deformation, offset tracking, SBAS-InSAR.**

I. Introduction

FOR a long time, coal has been China's main source of energy, supporting the national economic and social development [1]. However, coal mining has caused some ecological and environmental problems, which have seriously damaged surface buildings, farmland, roads, and water resources. The ground surface deformation is one of the major disasters caused by coal resource exploitation and it poses serious threats to the local people and environment [2]–[4]. Therefore, it is critical to monitor the surface subsidence caused by mining and determine the spatial size of the goaf to control mining subsidence damages effectively.

The traditional geodetic surveying methods, such as precision leveling, total station measurement, and global navigation satellite system, have played an important role in monitoring the surface deformation. However, with the continuous growth in deformation monitoring requirements and accuracy, the following defects of the traditional measurement methods are increasingly obvious:

1) large workload, long cycle, high cost, and low observation efficiency [5];
2) low spatial resolution, limited monitoring area, small amount of monitoring data, and inconvenience of obtaining 3-D spatial deformation and historical information; and
3) extreme difficulty in monitoring the surface deformation caused by large-scale, all-round, and multienvironmental factors. In particular, the monitoring effect is very poor in regions with large topographic fluctuations [6].

In recent years, remote sensing technology, especially the synthetic aperture radar interferometry (InSAR) technology, has become an important tool to monitor the ground surface displacement caused by tectonic and human activities given its low cost, strong penetrating ability, high precision and efficiency, and high spatio-temporal resolution [7]–[9]. In comparison with the traditional geodetic deformation monitoring technologies, InSAR can monitor long-term continuous surface displacements with centimeter-scale accuracy and detect a large-scale ground deformation under any weather conditions. Owning to these significant advantages, the InSAR technology is widely used to monitor mining subsidence [10], [11], volcanic activity [12], [13], landslide disasters [14]–[16], seismic deformation [17]–[19], urban deformation [20], and glacier surface movement [21]. However, the conventional InSAR method cannot effectively estimate the atmospheric delay phase and is easily constrained by the temporal and spatial decorrelation during the process of interference. In addition, the influences of the terrain residual error introduced by inaccurate digital elevation models (DEMs), orbital residual errors introduced by inaccurate orbit data, and phase unwrapping errors are inevitable [8], [22], [23].

Manuscript received April 18, 2020; revised September 5, 2020; accepted September 27, 2020. Date of publication October 1, 2020; date of current version October 15, 2020. This work was supported in part by the Natural Science Foundation of China under Grant 41804013, in part by the Natural Science Foundation of Jiangsu Province under Grant BK20180666, and in part by China Postdoctoral Science Foundation under Grant 2019M661988. *(Corresponding author: Kun Tan.)*

Yu Chen and Yunxiao Tong are with the Key Laboratory for Land Environment and Disaster Monitoring, Ministry of Natural Resources, China University of Mining and Technology, Xuzhou 221116, China (e-mail: chenyu@cumt.edu.cn; tyunxiao@126.com).

Kun Tan is with the Key Laboratory of Geographic Information Science, Ministry of Education, East China Normal University, Shanghai 200241, China (e-mail: tankuncu@gmail.com).

Digital Object Identifier 10.1109/JSTARS.2020.3028083

These factors have seriously affected the accuracy and reliability of the InSAR technology.

To overcome the above-mentioned shortcomings of the traditional InSAR technology, advanced multitemporal InSAR (MT-InSAR) technologies [24], which can effectively suppress the atmospheric delay phase and DEM error, have been proposed by domestic and foreign scholars to improve the accuracy and reliability of deformation monitoring. These include persistent scatterer InSAR [25], small baseline subset InSAR [26], interferometric point target analysis [27], and temporarily coherent point InSAR [28]. These MT-InSAR technologies can solve the problem of the spatio-temporal decorrelation by using permanent scatterers, which can maintain the phase and amplitude stability in multiview SAR images over a long period, thus enabling the monitoring accuracy of the surface deformation to reach centimeter- or even millimeter-level. However, owing to complex topography, multivegetation coverage, and large-scale deformation in a relatively short period of time, it is difficult to monitor the deformation of mining areas using conventional MT-InSAR technologies [29].

With the rapid development in the space SAR technology and significant improvement in SAR image pixel resolution, the pixel offset tracking technology based on the SAR image intensity information has received increasing attention in the deformation monitoring [30]. The offset tracking technology does not require phase unwrapping and can effectively reduce the effect of temporal and spatial decorrelation [31], [32]. Therefore, it has achieved good results in monitoring glacier motion [32], [33], seismic activity [34]–[36], and landslide movements [37]–[39]. More importantly, the improved offset tracking technology has been used to monitor the large-gradient subsidence of mining areas and has achieved a relatively reliable accuracy.

In the study, we aim to monitor the surface subsidence of mining areas using TerraSAR-X and Sentinel-1 SAR images based on the SBAS-InSAR and pixel offset tracking technologies. First, the TerraSAR-X and Sentinel-1 images with similar time spans were combined to detect surface subsidence in the mining area of Yu County. This approach not only preserves the high resolution of TerraSAR-X and greater monitoring capability of Sentinel-1 but also shortens the monitoring cycle. In addition, a fusion method is proposed to capitalize on the advantages of the MT-InSAR technology for high precision and of the offset tracking technology for the large-scale deformation monitoring. Moreover, the mining area of Yu County is one of the most typical and complex mining areas in China. It is geologically located at the intersection of two tectonic zones. Thus, the geological structure is complicated in this area. Ground fissures, subsidence, and even collapse all occurred in the mining history. According to our field investigation, many people are still residents in this area and few of their houses are built from reinforced concrete. Therefore, the uneven ground surface subsidence induced by mining activities is liable to cause a safety accident, e.g., wall cracking, which can cause great life and property losses. Hence, it is essential to regularly monitor the surface subsidence in this area. Up to now, the surface deformation situation in the study area has rarely been observed by InSAR and offset tracking techniques. Therefore, the monitoring results derived in this study can provide an important reference for disaster prevention and overall planning in mining areas.

II. Study Area and Data Used

The research area covers the Cuijiazhai and Danhou Coal Mines, encompassing an area of approximately 72 km^2, and its geographical coordinates are 114°26′38″E–114°32′46″E, 39°52′15″N–39°59′35″N (see Fig. 1). The Cuijiazhai mine was established in October 1996 and has an annual production capacity of 1.8 million tons and an area of 34 km^2. The Danhou mine was built in May 2004 and has an annual production capacity of 1.5 million tons and an area of 38 km^2.

To monitor and analyze the mining-induced displacement of the study area more comprehensively, the TerraSAR-X and Sentinel-1 SAR images, which cover the same study area and have almost synchronous time spans, were selected (see Table I). We used a total of 19 *X*-band SpotLight TerraSAR-X SAR images, covering the period from 20 June 2015 to 4 January 2016, using the descending pass with a revisit time of 11 days (providing valuable SAR image sources with shorter temporal baselines), spatial resolution of 1.99 × 0.91 m in the azimuth and range directions (providing high-resolution and high-quality SAR images for monitoring the features in detail) with an incidence angle of 28.7°, and horizontal transmit and horizontal receive (HH) polarization. On the other hand, we additionally acquired a series of 16 ascending C-band Sentinel-1 single look complex images from 17 June 2015 to 7 January 2016 in the interferometric wide (IW) swath mode with a mean incident angle of 37.5°, temporal baseline of 12 or 24 days, and vertical transmit and vertical receive (VV) polarization. The IW swath mode obtains three subswaths by using the terrain observation with progressive scans imaging mode covering a width of 250 km with a spatial resolution 2.3 × 13.9 m [40]. In addition, the shuttle radar topography mission DEM with a spatial resolution 1 arc·s (approximately 30 m), which is jointly measured by the National Aeronautics and Space Administration and National Imagery and Mapping Agency, was used to simulate the topographic phase and flat phase, and geocode the SAR images into geographic coordinates.

III. Methodology

A. SBAS-InSAR Processing

The DORIS and GAMMA software were first used to generate the differential interferograms for the TerraSAR-X and Sentinel-1 images, respectively. The SBAS-InSAR processing was then carried out using the Stanford method for persistent scatterers software package [41]. Debursting was applied to each Sentinel-1 image before the interferogram generation. The range and azimuth filtering was applied to both the datasets to reduce geometric decorrelation and discard nonoverlapping Doppler frequencies [42]. To suppress speckle noise and improve the signal-to-noise ratio of the images, the multilook processing of

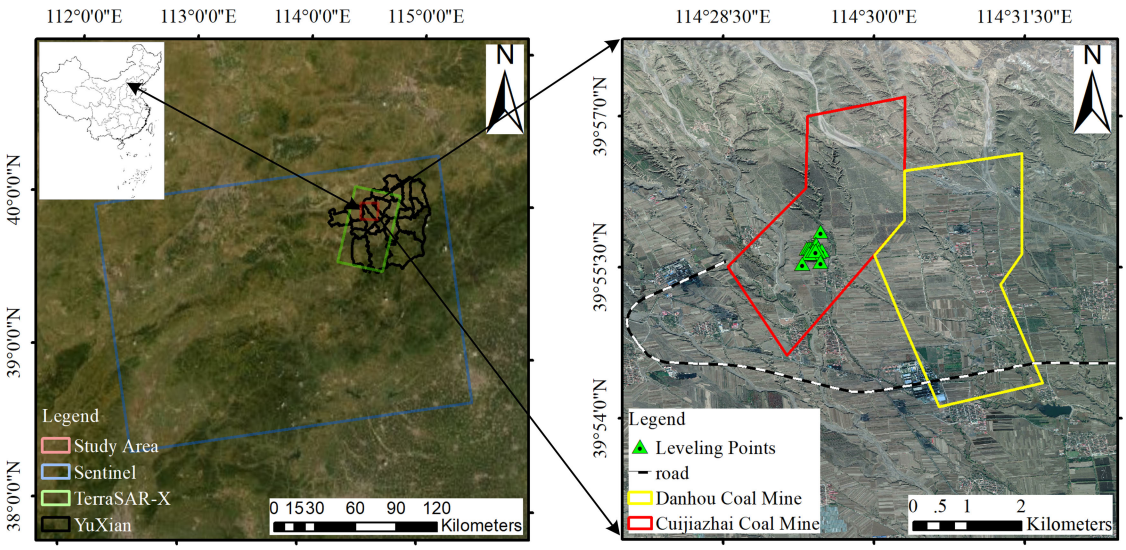

Fig. 1. Geographical location of research area in Yu County, China. The blue rectangle represents the coverage of ascending Sentinel-1 images. The green rectangle indicates the coverage of descending TerraSAR-X images. The black polygon represents the coverage of Yu County. The red rectangle represents the study area.

TABLE I
PARAMETERS OF TERRASAR-X AND SENTINEL-1 IMAGES

No.	Parameters	TerraSAR-X	Sentinel-1
1	Time span	20 June 2015– 04 January 2016	17 June 2015– 07 January 2016
2	Imaging mode	SpotLight	TOPS-IW
3	Spatial resolution	0.91×1.99	2.3×13.9
4	Pass way	Descending	Ascending
5	Revisit cycle(days)	11	12 or 24
6	Polarization	HH	VV
7	Incident angle	28.7°	37.5°
8	Orbit number	28	40
9	Wavelength(cm)	X-band 3.11	C-band 2.6

TOPS: Terrain observation with progressive scans.

10×10 and 5×1 in the range and azimuth directions were carried out for the TerraSAR-X and Sentinel-1 images, respectively. The topographic contribution was removed and the interferograms were georeferenced with the aid of the 30 m DEM. Two small baseline subsets (including 41 and 38 interferograms for the TerraSAR-X and Sentinel-1 datasets, respectively) were eventually constructed from interferograms with perpendicular baselines less than 550 m and temporal baselines shorter than 90 days for the TerraSAR-X images, and from interferograms with perpendicular baselines less than 400 m and temporal baselines shorter than 80 days for the Sentinel-1 images (see Fig. 2).

The coherent pixels referred to as slowly-decorrelating filtered phase (SDFP) pixels were extracted according to a criterion based on a combination of coherence coefficient and amplitude stability [43]. The 3-D unwrapping algorithm [43], [44], which takes "time" into consideration (as the third dimension) was used to unwrap the phases of the SDFP pixels. We used a linear empirical function to estimate the phase ramps induced by orbit errors and atmospheric delays. The displacement time series corresponding to each SAR acquisition was inverted using a least squares adjustment after the estimation and removal of the baseline-dependent residuals induced by the errors in the DEM.

B. *Offset Tracking*

Although the conventional D-InSAR and MT-InSAR technologies have high deformation monitoring accuracies of up to the centimeter- or even millimeter-level, they are largely limited by the spatio-temporal coherence and deformation gradients. It is extremely difficult to reconstruct the reliable and accurate surface deformation information in the case of the large-gradient subsidence in mining areas using InSAR technologies. Therefore, increasing attention is being paid to the offset tracking technique, which uses the amplitude information of the SAR

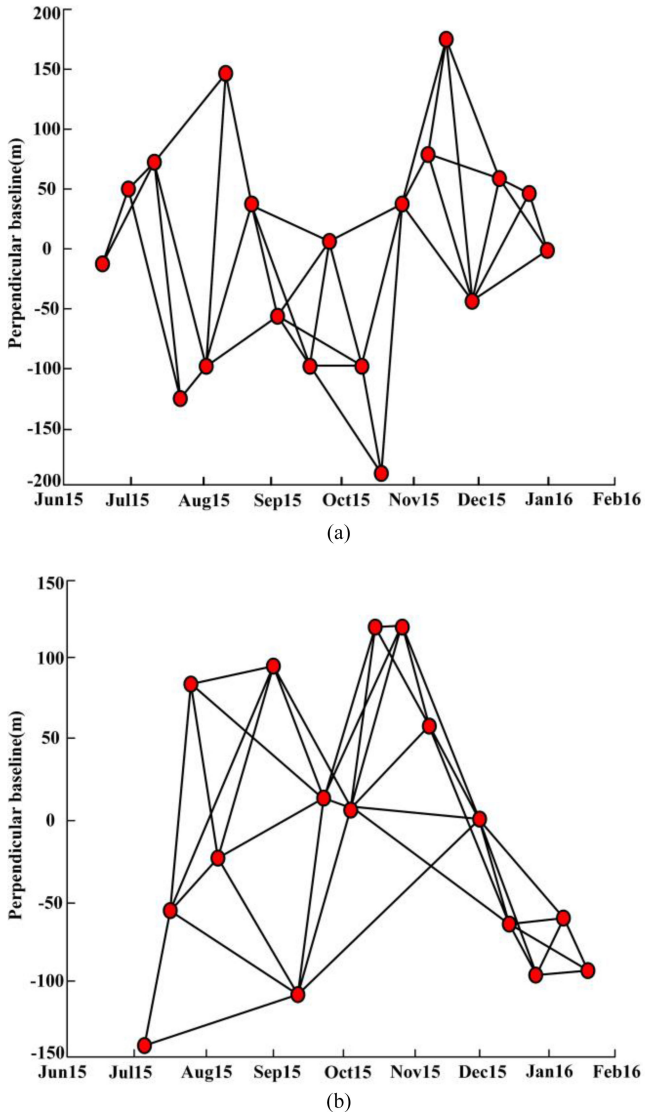

Fig. 2. Perpendicular and temporal baseline distributions of the small baseline subsets for (a) TerraSAR-X and (b) Sentinel-1 datasets. Red dots indicate the SAR images and black lines represent the interferograms formed from the two corresponding SAR images.

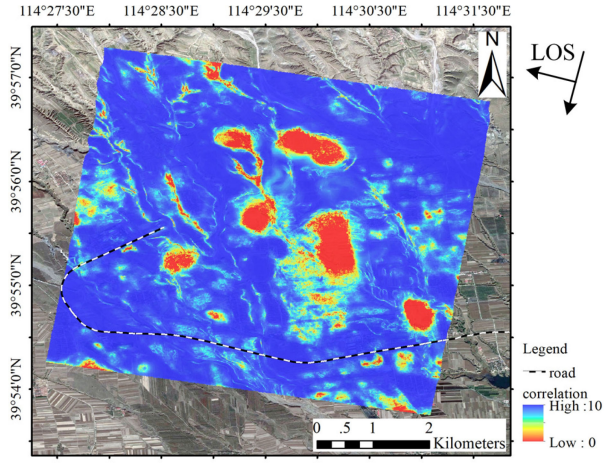

Fig. 3. Total spatial coherence distribution map with values in the range 0–10.

images [45], [46]. The highest theoretical monitoring precision of the offset tracking technique can reach approximately 3.3 cm for TerraSAR-X images with a spatial resolution of 0.91 × 1.99 m in the azimuth and range directions, which can effectively compensate for the defects of the InSAR methods in large-scale deformation applications [47], [48].

In the present study, the offset tracking processing was implemented using the GAMMA software. To reduce the terrain fluctuation and image registration errors, an imaging pair (images acquired on 20 June 2015 and 4 January 2016) with a small perpendicular baseline (12.58 m) was selected from the TerraSAR-X dataset. The initial pixel offset was obtained via coarse registration based on the orbital parameter files of the primary and auxiliary images. The subpixel offset was achieved via accurate registration based on a certain search window and normalized cross-correlation algorithm based on the initial offset. An oversampling was additionally applied to obtain the final subpixel offset. Compared with the phase information, the intensity is more stable in the study area with a large vegetation cover. Therefore, the offset tracking method based on the intensity information was adopted to monitor the large-gradient deformation in this study. Based on numerous pixel offset tracking experiments, the optimal parameters were established as follows: the search window of 256 × 256, step factor of 1, and oversampling factor of 4.

C. Decision Fusion Algorithm

Considering the high-precision advantages of the SBAS-InSAR technology in the field of small-scale deformation and the strong potential of the offset tracking technique in the field of large-scale deformation, a decision fusion method combining the results of SBAS-InSAR and offset tracking was developed based on the total spatial coherence map.

Specifically, the coherence coefficient maps were first generated during each process of interference. They were then superimposed to obtain a total spatial coherence distribution map, as shown in Fig. 3. The values of total spatial coherence were normalized to 0–10. The higher the value, the higher the coherence. The results of SBAS-InSAR and pixel offset tracking are then fused based on the total spatial coherence map, according to the following fusion algorithm:

$$\text{Final deformation result} = \begin{cases} \mathrm{X}, \text{ if } \mathrm{Z} \geq T_h \text{ or } \mathrm{Y} = 0 \\ \mathrm{Y}, \text{ if } \mathrm{Z} < T_l \text{ and } X_{\min} > \mathrm{Y} \\ \mathrm{X}, \text{ else if } T_l \leq \mathrm{Z} < T_h \text{ and } \mathrm{X} < \mathrm{Y} \\ \frac{\mathrm{Z}}{\mathrm{Z}_{\max}}\mathrm{X} + \frac{\mathrm{Z}_{\max}-\mathrm{Z}}{\mathrm{Z}_{\max}}\mathrm{Y}, \text{ else} \end{cases} \quad (1)$$

where X represents the deformation results obtained by SBAS-InSAR, Y represents the deformation results obtained by the offset tracking technology, and Z represents the total spatial coherence distribution map. T_h and T_l are two coherence thresholds. The total coherence value greater than or equal to T_h indicates that the InSAR coherence was good. A value lower than

T_l indicates serious decoherence or even complete decoherence. The detailed descriptions are given as follows.

1) When the value of the spatial coherence map, *Z*, was greater than or equal to T_h, the SBAS-InSAR technique could obtain more accurate and reliable deformation information owing to a good coherence in space and time. Therefore, the result, *X*, obtained by the SBAS-InSAR method directly serves as the final deformation monitoring result of the mining area.
2) The displacement result obtained by the pixel offset tracking technique was zero owing to a low registration accuracy. Hence, the SBAS-InSAR result, *X*, was used as the final deformation result.
3) When the value of the spatial coherence map, *Z*, was less than T_l and the offset tracking result, *Y*, was lower than the minimum SBAS-InSAR result, *X*, the former, i.e., the offset tracking result, was used as the final fusion result. The pixel offset tracking technique was superior to the SBAS-InSAR technique in the case of severe spatio-temporal decoherence caused by the large-scale deformation.
4) When the value of the spatial coherence map, *Z*, was greater than or equal to T_l and less than T_h, and the SBAS-InSAR result, *X*, was less than the offset tracking result, *Y*, the SBAS-InSAR monitoring deformation result was used as the final fusion result. If the spatio-temporal decoherence was not particularly serious, the SBAS-InSAR technique had higher accuracy and reliability than those of the offset tracking method. Moreover, the coal mining area we studied was characterized by land subsidence as the main surface activity. Hence, we adopted the SBAS-InSAR result when the SBAS result was negative and the offset tracking result when the SBAS result was negative.
5) In other cases, we adopted the proportional method to consider comprehensively the SBAS-InSAR and pixel offset tracking results to improve the reliability of the deformation result to the maximum possible extent.

As above mentioned, the proposed fusion algorithm is mainly based on two coherence thresholds ($T_h$and T_l) indicating the critical reliability level of the measurements derived from SBAS-InSAR and offset tracking techniques. Therefore, we took particular caution when selecting them. First, the visual inspections (repeated comparisons between the total coherence map and the deformation results) showed that the InSAR coherence was good when T_h was around 7–9 and it showed serious decoherence or even complete decoherence when T_l was around 4–5. Then we fixed T_l, e.g., 5, and adjusted T_h from 7 to 9 with a step length of 0.5 to search the most appropriate value that led to a minimum mean absolute error between the leveling measurements and fusion results. Then we fixed T_h, e.g., 8, and adjusted T_l from 4 to 5 similarly. Repeated experiments showed that, on one hand, when $T_h = 8.5$ or 9, many pixels with a good InSAR coherence were distributed to the proportional combination part. The participation of the offset tracking measurements would affect the reliability of the fusion result. One the other hand, when T_h was lower than 8, the proportion of InSAR measurements in the fusion results would be so large that the subsidence might be underestimated according to the differences between the leveling measurements and fusion results. It was also found that the mean absolute error between the leveling measurements and fusion results was the lowest when T_l was equal to 5. Therefore, 8 and 5 were assigned to T_h and T_l, respectively.

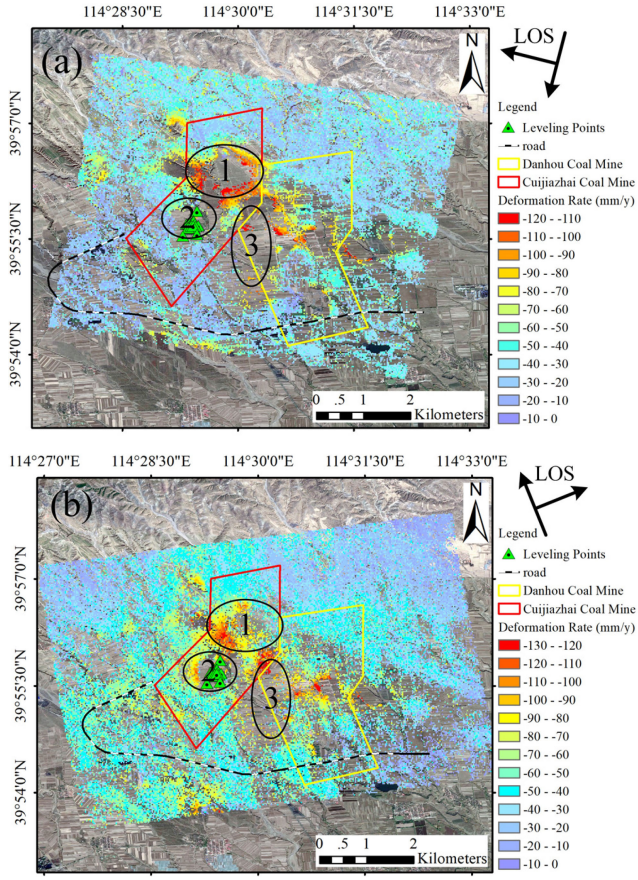

Fig. 4. Mean displacement rates in LOS for study area from (a) TerraSAR-X time series (20 June 2015–4 January 2016) and (b) Sentinel-1 time series (17 June 2015–7 January 2016).

IV. Results

A. Displacement Rates in Line-of-Sight and in Vertical/East–West Directions

The mean displacement rates in the line-of-sight (LOS) direction for the *X*-band TerraSAR-X and *C*-band Sentinel-1 datasets are shown in Fig. 4. The color of the selected high coherence points from blue to red indicates a gradual increase in displacement rates. Fig. 4 shows that the results derived from the two datasets coincide in terms of their deformation spatial patterns. The phenomenon of surface subsidence appeared in most of the study area. In particular, three subsidence funnels located in the Cuijiazhai and Danhou Coal Mines, indicated by the ellipses 1–3, owing to the massive mining of coal resources are obviously present. The maximum surface subsidence rate in the research area is approximately 125 mm/y in the LOS direction. To render the two datasets comparable and consistent for further processing, they were resampled to the same resolution (15 m). A visual inspection showed that the numbers of coherent points

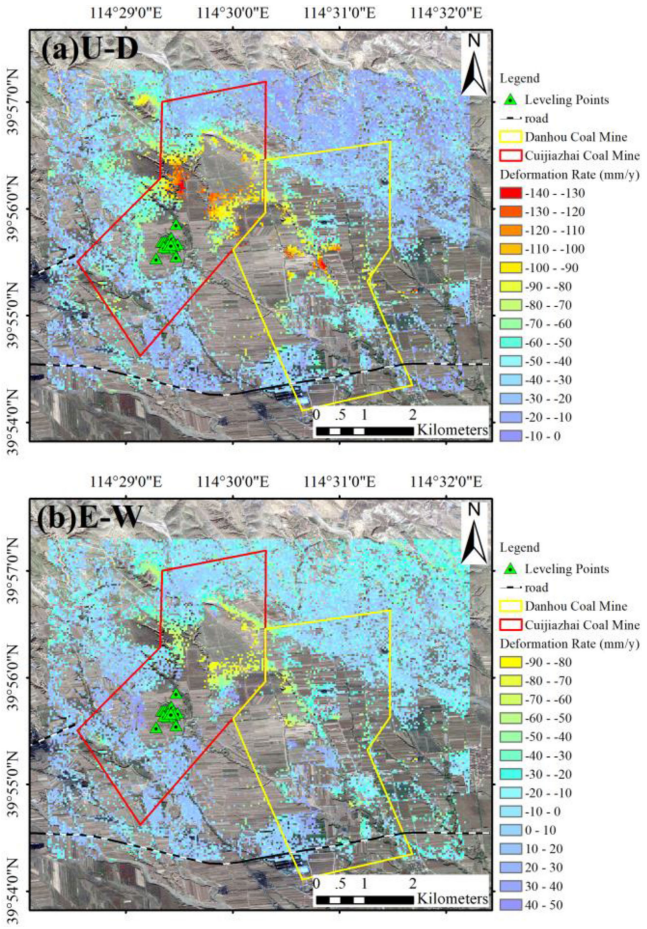

Fig. 5. (a) U-D and (b) E–W components of displacement rates for the study area from two SAR datasets with different viewing geometries. Negative values indicate subsidence in (a) and westward displacement in (b).

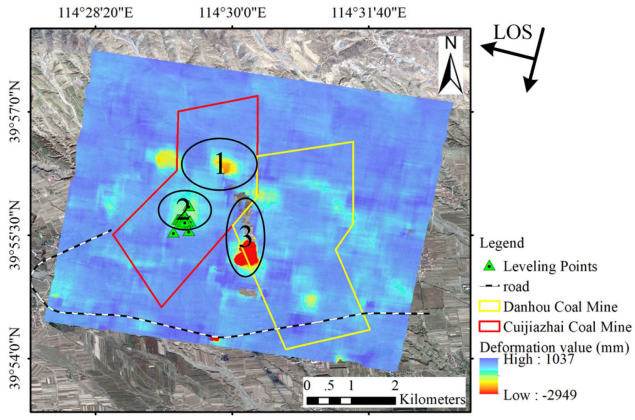

Fig. 6. Result of pixel offset tracking using TerraSAR-X images for 20 June 2015 and 4 January 2016.

remaining in the two maps were clearly different. More coherent points remained in the Sentinel-1 data, particularly in the large-gradient deformation areas. This is because the maximum monitoring range is closely related to the radar operating wavelength (half of the wavelength). The long-wavelength *C*-band radar wave has more potential than the *X*-band wave to detect the large-gradient deformation. Nevertheless, the deformation gradients in the central parts of the subsidence funnels induced by the high mining intensity of the mining areas exceeded the monitoring abilities of both the *C*- and *X*-band waves, resulting in insufficient coherent points in the region of interest. For instance, the leveling points were mostly located within the subsidence funnel 2, where, unfortunately, no coherent point was obtained owing to the extremely large deformation gradient.

The different viewing geometries of the two SAR datasets allowed us to map the surface displacement rates in two dimensions [vertical (U-D) and east–west (E–W) components], as shown in Fig. 5. We selected the common points between the displacement rate maps of the two datasets, which means that the tradeoff is the loss of a certain number of coherent points. Fig. 5(a) shows the average displacement rates in the U-D direction. The surface subsidence was particularly obvious in the vertical directions of the Cuijiazhai and Danhou Coal Mines, and the maximum surface subsidence rate was 140 mm/y. Fig. 5(b) represents the average displacement rates in the E–W direction. It shows that the main deformation in the Cuijiazhai and Danhou Coal Mines occurred in the western direction, and the maximum displacement rate was approximately 90 mm/y.

B. Results of Offset Tracking

Fig. 6 illustrates the experimental results of offset tracking using the TerraSAR-X data. Several serious subsidence funnels owing to the massive exploitation of coal resources are evident. Compared with the deformation results derived by the SBAS-InSAR method in Fig. 4, evidently more subsidence information was obtained by the offset tracking method in the elliptical zones 1–3 where the InSAR time series technique failed to retain sufficient coherent points. This indicates that the offset tracking is more capable of monitoring large-gradient displacement in mining areas. The lack of obvious features reduces the accuracy of image registration, resulting in a blank area without deformation information in the elliptical zone 3. The monitoring results of the pixel tracking method show that the maximum subsidence was approximately 2950 mm (near the elliptical zone 3) in the Yu County Coal Mine area from June 2015 to January 2016. The remaining subsidence funnels show a relatively lower displacement in the range 560–1210 mm. These results show that the massive exploitation of coal resources resulted in severe surface subsidence in the mining area and caused serious destruction to the surrounding environment during the study period.

C. Fusion Result of SBAS-InSAR and Offset Tracking

Fig. 7 shows the fusion results of SBAS-InSAR and pixel offset tracking for the TerraSAR-X data. It can be seen that the fusion results compensate for the shortcomings of the monitoring results using the SBAS-InSAR method in isolation as the map reflects both the slight displacement and high-gradient displacement information. The accuracy and reliability of the fusion results were verified using the nearest precise leveling data, as given in Table II. At some individual points, there

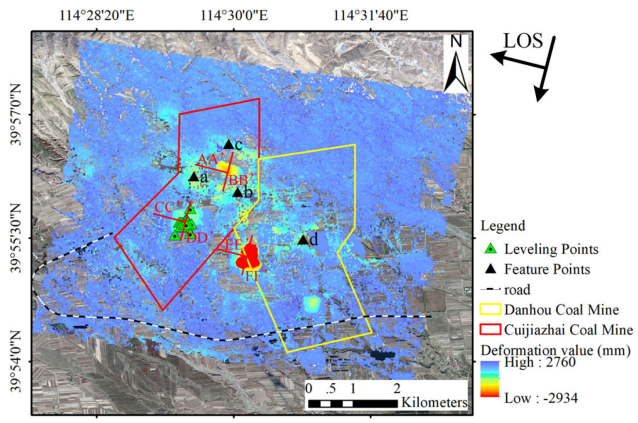

Fig. 7. Fusion result of SBAS-InSAR and pixel offset tracking.

TABLE II
COMPARISON OF LEVELING RESULT AND FUSION RESULT OF SBAS-INSAR AND OFFSET TRACKING IN LOS DIRECTION (MM)

No.	Leveling(LOS)	Fusion Result	Absolute Error
S01	650.6	584.6	66.0
S02	841.1	735.6	105.5
S03	585.3	523.9	61.4
S04	381.8	334.9	46.9
S05	704.5	622.3	82.2
S06	748.8	631.5	117.3
S07	759.2	690.7	68.5
S08	877.4	783.5	93.9
S09	894.0	847.2	46.8
S10	905.1	752.8	152.3
S11	898.0	803.1	94.9
S12	777.2	807.9	-30.7
S13	110.3	120.3	-10.0
S14	65.7	68.2	-2.5
S15	66.2	69.7	-3.5
Mean	617.7	558.4	59.3

are greater differences between the leveling result and fusion result, which may be owing to the image registration errors or temporal differences. The average absolute error of the leveling and fusion results is approximately 59.3 mm, which indicates that the fusion result has a higher precision in large-gradient deformation regions.

Fig. 8 shows the displacement time series for four feature points *a*–*d*. (Points *a*–*c* are located in the north Cuijiazhai Coal Mine area and point *d* is located in the central Danhou Coal Mine area.) It can be seen that the temporal evolution of subsidence at these points can be described approximately by linear trends with the average subsidence rates of −94.02, −110.61, −82.96, and −68.21 mm/y, respectively.

Fig. 9 shows some deformation profiles of the elliptical zones 1–3 in the direction of LOS and perpendicular to LOS (red line in Fig. 7). It can be clearly seen from Fig. 9 that in the

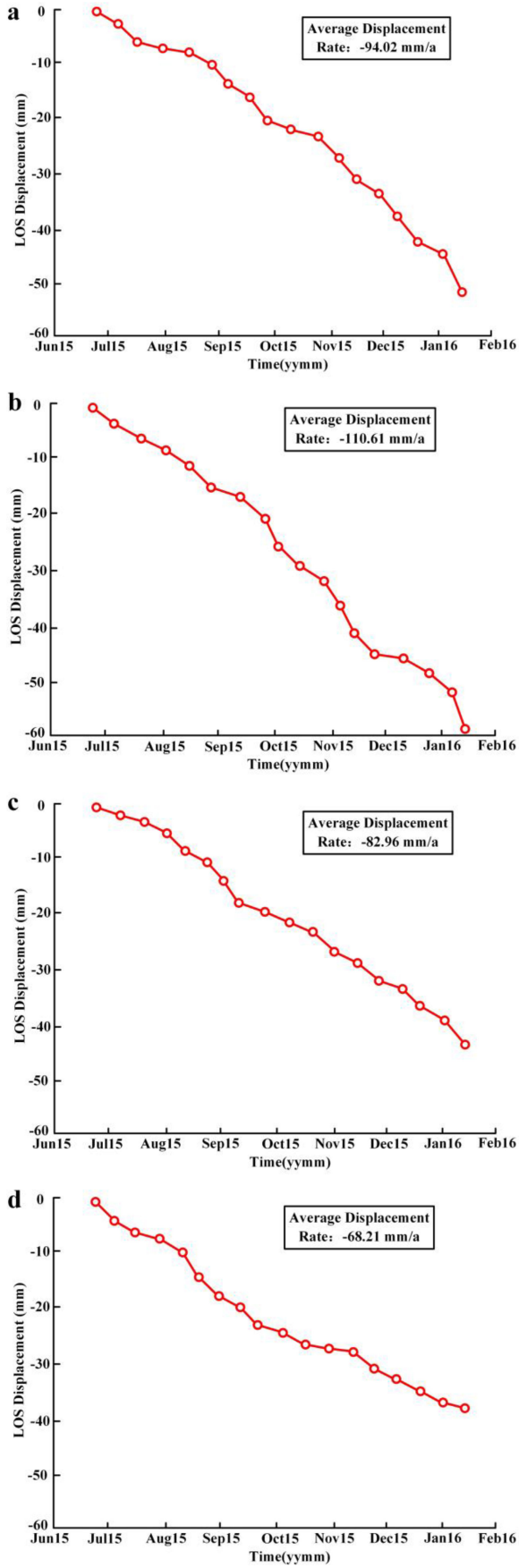

Fig. 8. Displacement time series for four feature points *a*–*d*. Locations of feature points are marked in Fig. 7.

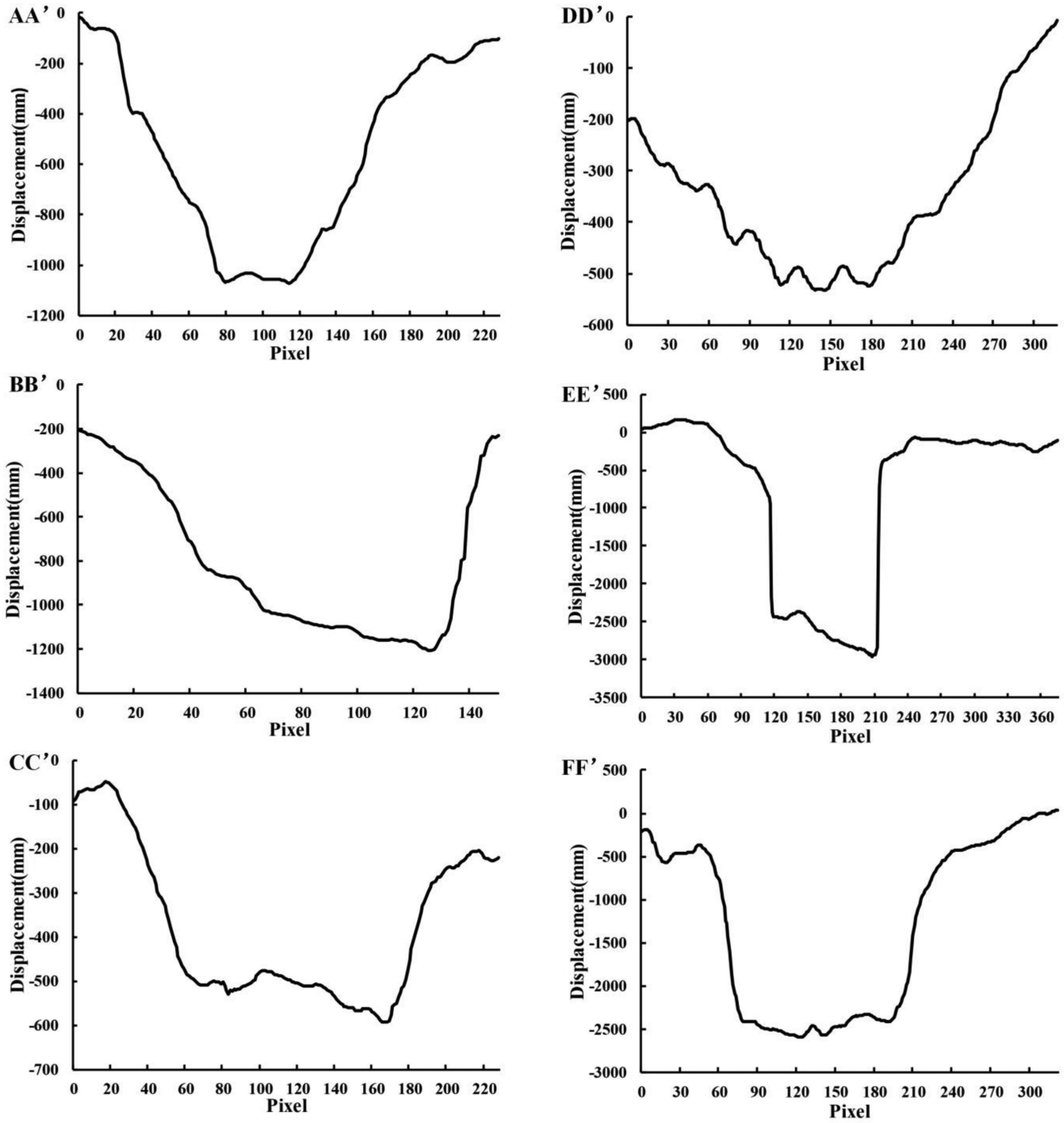

Fig. 9. Deformation profiles located in elliptical zones 1–3 (see Fig. 7 for locations).

elliptical zones 1–3, serious settlement funnels have formed in both the direction of LOS and perpendicular to LOS owing to the large-scale mining of coal resources. More specifically, severe surface subsidence occurred in the elliptical zone 1 with a maximum deformation of approximately 1100 mm and relatively slight ground subsidence occurred in the elliptical zone 2 with a maximum deformation of approximately 550 mm. The most serious surface subsidence occurred in the elliptical zone 3 with a maximum deformation of approximately 3000 mm.

V. Discussion

A. Limitation of SAR Data

The original purpose of this study was to obtain the 3-D deformation information of the Yu County Coal Mine area. As is well known, the SAR satellite data from a minimum of three different orbits are required to reconstruct the real 3-D deformation results. However, the SAR satellite data available in the study area are only the TerraSAR-X images of the descending

orbit and the Sentinel-1 images of the ascending orbit. Unfortunately, the Sentinel-1 images of the descending orbit cannot be obtained. Considering that the SAR image is insensitive to the north–south deformation, the TerraSAR-X and Sentinel-1 images were used to capture the deformation results in the U-D and E–W directions.

It is unreasonable to deduce that most of the level verification points are located in the elliptical zone 2 with large deformation as a result of the insufficient preliminary investigation. It is indeed difficult for the SBAS-InSAR technology to capture the deformation information in the elliptical zone 2 as the surface subsidence gradient of the mining area is greater than the monitoring capability of the technology. Therefore, the inversion result of the offset tracking technology was used to compare and verify the results of SBAS-InSAR. Furthermore, several regions with no expected deformation were selected to verify the reliability of the fusion result. The standard deviation was less than 8 mm in all the regions and the average standard deviation was 5.56 mm. To some extent, the reliability of the SBAS and fusion results is verified.

B. Condition of Offset Tracking Experiment

We tried our best to use the Sentinel-1 images for the offset tracking experiment and then carried out the fusion experiment with SBAS similar to that with the TerraSAR-X images. In that case, we would have been able to obtain the fusion results in 2 D, which would have largely strengthened the content and structure of this article. However, after many experiments, the use of Sentinel-1 images to retrieve the offset tracking results remained unsuccessful. In our analysis, there are a few reasons for the failure of the offset tracking experiment. First, the accuracy of the experiment is closely related to the spatial resolution of the SAR images. Compared with the TerraSAR data, the lower spatial resolution characteristic of the Sentinel-1 images may have been a cause of failure, especially when the deformation affecting area is small. Second, the land cover and weather conditions vary greatly in the study area. Crops and bushes that have unstable backscattering characteristics are the main land cover types around the mining area. In addition, the study time period spans from summer to winter. In late 2015 and early 2016 when we conducted a field investigation, the study area was covered with thick snow. The above-mentioned factors may have significantly affected the textural features of SAR images. There may have been errors in the identification of homonymous image points on the primary and secondary images owing to the lack of particularly obvious features in the study area, which may have led to the failure. Third, the registration accuracy of the primary and secondary SAR images is an additional key factor determining the success or failure of the offset tracking experiment. Hence, the low quality of image registration may have been another cause of the failure. The relatively low signal-to-noise ratio of the Sentinel-1 images may have been the fourth affecting factor leading to unreliable results. Determining the exact cause of the failure of the offset tracking experiment using Sentinel-1 images is the focus of future research.

VI. Conclusion

In this study, the TerraSAR-X and Sentinel-1 images were used to determine the ground deformation in the Yu County Coal Mine area, China, based on SBAS-InSAR with the high precision and pixel offset tracking with the large-gradient deformation monitoring capability from 20 June 2015 to 4 January 2016. Comparing the surface subsidence results of SBAS-InSAR from TerraSAR-X and Sentinel-1 data, it is seen that the conventional SBAS-InSAR technique shows superior performance in mining regions with the small-scale deformation. However, the SBAS-InSAR method cannot easily detect reliable displacement information in the large-scale deformation areas as a result of the interferometric phase decorrelation caused by the large subsidence gradient. In addition, the pixel offset tracking technology based on the intensity information of SAR images requires subpixel registration accuracy and estimates the surface deformation from the subpixel offset, which can compensate for the shortcomings of the SBAS-InSAR technology in the large-scale deformation.

This study realized the purpose of monitoring the large-gradient ground subsidence of the mining area by combining the respective advantages of the SBAS-InSAR and offset tracking technologies. From the results of SBAS-InSAR and offset tracking, it was determined that the large-gradient ground subsidence has occurred in the study area as a result of the massive mining of coal resources. The maximum subsidence rate is approximately 125 mm/y and the maximum settlement is approximately 2950 mm. The mean absolute error of the leveling and fusion results is approximately 59.3 mm, which indicates that the fusion method determined relatively reliable displacement information in large-scale deformation areas. Therefore, the comprehensive use of the phase information and intensity information of the SAR images enables us to monitor the large-gradient deformation with high accuracy and reliability by combining the SBAS-InSAR and offset tracking technologies. In addition, enough attention should be paid to the observed large-scale subsidence in the study area to prevent potential disasters. On one hand, it is of the greatest importance to monitor the surface subsidence at regular intervals using InSAR, offset tracking, and GNSS techniques, etc. On the other hand, improving the mining strategy may be considered when necessary to reduce the subsidence magnitude at the source.

References

[1] J. Wang, L. Feng, S. Davidsson, and M. Höök, "Chinese coal supply and future production outlooks," *Energy*, vol. 60, pp. 204–214, 2013.

[2] E. Chaussard, S. Wdowinski, E. Cabral-Cano, and F. Amelunga, "Land subsidence in central Mexico detected by ALOS InSAR time-series," *Remote Sens. Environ.*, vol. 140, pp. 94–106, 2014.

[3] K. Dai *et al.*, "Monitoring activity at the Daguangbao mega-landslide (China) using Sentinel-1 TOPS time series interferometry," *Remote Sens. Environ.*, vol. 186, pp. 501–513, 2016.

[4] X. Feng and Q. Zhang, "The effect of backfilling materials on the deformation of coal and rock strata containing multiple goaf: A numerical study," *Minerals*, vol. 8, no. 6, p. 224, 2018.

[5] Y. Xia, Y. Wang, S. Du, X. Liu, and H. Zhou, "Integration of D-InSAR and GIS technology for identifying illegal underground mining in Yangquan District, Shanxi Province, China," *Environ. Earth Sci.*, vol. 77, no. 8, p. 319, 2018.

[6] C. Liu, F. Zhou, J. Gao, and J. Wang, "Some problems of GPS RTK technique application to mining subsidence monitoring," *Int. J. Mining Sci. Technol.*, vol. 22, no. 2, pp. 223–228, 2012.

[7] P. A. Rosen *et al.*, "Synthetic aperture radar interferometry," *Proc. IEEE*, vol. 88, no. 3, pp. 333–382, Mar. 2000.

[8] Z. F. Yang, Z. W. Li, J. J. Zhu, J. Hu, Y. J. Wang, and G. L. Chen, "InSAR-based model parameter estimation of probability integral method and its application for predicting mining-induced horizontal and vertical displacements," *IEEE Trans. Geosci. Remote Sens.*, vol. 54, no. 8, pp. 4818–4832, Aug. 2016.

[9] Y. Du, L. Zhang, G. Feng, Z. Lu, and Q. Sun, "On the accuracy of topographic residuals retrieved by MTInSAR," *IEEE Trans. Geosci. Remote Sens.*, vol. 55, no. 2, pp. 1053–1065, Feb. 2017.

[10] L. Jiang, H. Lin, J. Ma, B. Kong, and Y. Wang, "Potential of small-baseline SAR interferometry for monitoring land subsidence related to underground coal fires: Wuda (Northern China) case study," *Remote Sens. Environ.*, vol. 115, no. 2, pp. 257–268, 2011.

[11] D. Ou, K. Tan, Q. Du, Y. Chen, and J. Ding, "Decision fusion of D-InSAR and pixel offset tracking for coal mining deformation monitoring," *Remote Sens.*, vol. 10, no. 7, p. 1055, 2018.

[12] A. Pavez *et al.*, "Insight into ground deformations at Lascar volcano (Chile) from SAR interferometry, photogrammetry and GPS data: Implications on volcano dynamics and future space monitoring," *Remote Sens. Environ.*, vol. 100, no. 3, pp. 307–320, 2006.

[13] Y. Chen *et al.*, "Long-term ground displacement observations using InSAR and GNSS at Piton de la Fournaise volcano between 2009 and 2014," *Remote Sens. Environ.*, vol. 194, pp. 230–247, 2017.

[14] J. Dong *et al.*, "Mapping landslide surface displacements with time series SAR interferometry by combining persistent and distributed scatterers: A case study of Jiaju landslide in Danba, China," *Remote Sens. Environ.*, vol. 205, pp. 180–198, 2018.

[15] F. Zhao, J. J. Mallorqui, R. Iglesias, K. A. Gili, and J. Corominas, "Landslide monitoring using multi-temporal SAR interferometry with advanced persistent scatterers identification methods and super high-spatial resolution TerraSAR-X images," *Remote Sens.*, vol. 10, no. 6, p. 921, 2018.

[16] X. Hu, Z. Lu, T. C. Pierson, R. Kramer, and D. L. George, "Combining InSAR and GPS to determine transient movement and thickness of a seasonally active low-gradient translational landslide," *Geophys. Res. Lett.*, vol. 45, pp. 1453–1462, 2018.

[17] W.-J. Lee, Z. Lu, H.-S. Jung, and L. Ji, "Measurement of small co-seismic deformation field from multi-temporal SAR interferometry: Application to the 19 September 2004 Huntoon Valley earthquake," *Geomatics, Natural Hazards Risk*, vol. 8, no. 2, pp. 1241–1257, 2017.

[18] Z. Wang, R. Zhang, X. Wang, and G. Liu, "Retrieving three-dimensional co-seismic deformation of the 2017 MW 7. 3 Iraq earthquake by multi-sensor SAR images," *Remote Sens.*, vol. 10, no. 6, p. 857, 2018.

[19] D. Massonnet *et al.*, "The displacement field of the Landers earthquake mapped by radar interferometry," *Nature*, vol. 364, pp. 138–142, 1993.

[20] Y. Chen *et al.*, "Monitoring land surface displacement over Xuzhou (China) in 2015–2018 through PCA-based correction applied to SAR interferometry," *Remote Sens.*, vol. 11, no. 12, p. 1494, 2019.

[21] G. Li, H. Lin, and Q. Ye, "Heterogeneous decadal glacier downwasting at the Mt. Everest (Qomolangma) from 2000 to 2012 based on multi-baseline bistatic SAR interferometry," *Remote Sens. Environ.*, vol. 206, pp. 336–349, 2018.

[22] C. Zhao, Z. Lu, Q. Zhang, C. Yang, and W. Zhu, "Mining collapse monitoring with SAR imagery data: A case study of Datong mine, China," *J. Appl. Remote Sens.*, vol. 8, no. 1, p. 083574, 2014.

[23] H. Yu, Y. Lan, Z. Yuan, J. Xu, and H. Lee, "Phase unwrapping in InSAR: A review," *IEEE Geosci. Remote Sens. Mag.*, vol. 7, no. 1, pp. 40–58, Mar. 2019.

[24] F. Xue, X. Lv, F. Dou, and Y. Yun, "A review of time-series interferometric SAR techniques: A tutorial for surface deformation analysis," *IEEE Geosci. Remote Sens. Mag.*, vol. 8, no. 1, pp. 22–42, Mar. 2020.

[25] A. Hooper, H. Zebker, P. Segall, and B. Kampes, "A new method for measuring deformation on volcanoes and other natural terrains using InSAR persistent scatterers," *Geophys. Res. Lett.*, vol. 31, no. 23, 2004, Art. no. L23611.

[26] P. Berardino, G. Fornaro, R. Lanari, and E. Sansosti, "A new algorithm for surface deformation monitoring based on small baseline differential SAR interferograms," *IEEE Trans. Geosci. Remote Sens.*, vol. 40, no. 11, pp. 2375–2383, Nov. 2002.

[27] C. Werner, U. Wegmuller, T. Strozzi, and A. Wiesmann, "Interferometric point target analysis for deformation mapping," in *Proc. IEEE Int. Geosci. Remote Sens. Symp.*, 2003, pp. 4362–4364.

[28] L. Zhang, Z. Lu, X. Ding, H.-S. Jung, G. Feng, and C.-W. Lee, "Mapping ground surface deformation using temporarily coherent point SAR interferometry: Application to Los Angeles Basin," *Remote Sens. Environ.*, vol. 117, pp. 429–439, 2012.

[29] Z. Yang, Z. Li, J. Zhu, H. Yi, J. Hu, and G. Feng, "Deriving dynamic subsidence of coal mining areas using InSAR and logistic model," *Remote Sens.*, vol. 9, no. 2, 2017.

[30] G. A. Arciniegas, W. Bijker, N. Kerle, and V. A. Tolpekin, "Coherence- and amplitude-based analysis of seismogenic damage in bam, Iran, using ENVISAT ASAR data," *IEEE Trans. Geosci. Remote Sens.*, vol. 45, no. 6, pp. 1571–1581, Jun. 2007.

[31] J. Cai, C. Wang, X. Mao, and Q. Wang, "An adaptive offset tracking method with SAR images for landslide displacement monitoring," *Remote Sens.*, vol. 9, no. 8, p. 830, 2017.

[32] P. Sánchez-Gámez and F J. Navarro, "Glacier surface velocity retrieval using D-InSAR and offset tracking techniques applied to ascending and descending passes of Sentinel-1 data for southern Ellesmere ice caps, Canadian Arctic," *Remote Sens.*, vol. 9, no. 5, p. 442, 2017.

[33] T. Strozzi, A. Kouraev, A. Wiesmann, U. Wegmüller, A. Sharov, and C. Werner, "Estimation of Arctic glacier motion with satellite L-band SAR data," *Remote Sens. Environ.*, vol. 112, no. 3, pp. 636–645, 2008.

[34] T. Wang and S. Jonsson, "Improved SAR amplitude image offset measurements for deriving three-dimensional coseismic displacements," *IEEE J. Sel. Topics Appl. Earth Observ.*, vol. 8, no. 7, pp. 3271–3278, Jul. 2015.

[35] B. Xu *et al.*, "Continent-wide 2-D co-seismic deformation of the 2015 Mw 8.3 Illapel, Chile earthquake derived from Sentinel-1A data: Correction of azimuth co-registration error," *Remote Sens.*, vol. 8, no. 5, p. 376, 2016.

[36] X. Hu, T. Wang, and M. Liao, "Measuring coseismic displacements with point-like targets offset tracking," *IEEE Geosci. Remote Sens. Lett.*, vol. 11, no. 1, pp. 283–287, Jan. 2014.

[37] A. Singleton, Z. Li, T. Hoey, and J.-P. Muller, "Evaluating sub-pixel offset techniques as an alternative to D-InSAR for monitoring episodic landslide movements in vegetated terrain," *Remote Sens. Environ.*, vol. 147, no. 9, pp. 133–144, 2014.

[38] M. Li, L. Zhang, X. Shi, M. Liao, and M. Yang, "Monitoring active motion of the Guobu landslide near the Laxiwa hydropower station in China by time-series point-like targets offset tracking," *Remote Sens. Environ.*, vol. 221, pp. 80–93, 2019.

[39] X. Hu, R. Burgmann, W. H. Schulz, and E. J. Fielding, "Four-dimensional surface motions of the Slumgullion landslide and quantification of hydrometeorological forcing," *Nature Commun.*, vol. 11, no. 1, p. 2792, 2020.

[40] N. Yagüe-Martínez *et al.*, "Interferometric processing of Sentinel-1 TOPS data," *IEEE Trans. Geosci. Remote Sens.*, vol. 54, no. 4, pp. 2220–2234, Apr. 2016.

[41] A. Hooper, D. Bekaert, K. Spaans, and M. Arikan, "Recent advances in SAR interferometry time series analysis for measuring crustal deformation," *Tectonophysics*, vol. 514/517, pp. 1–13, 2012.

[42] A. Hooper, "A multi-temporal InSAR method incorporating both persistent scatterer and small baseline approaches," *Geophys. Res. Lett.*, vol. 35, no. 16, 2008, Art. no. L16302.

[43] A. Hooper and H. A. Zebker, "Phase unwrapping in three dimensions with application to InSAR time series," *J. Opt. Soc. Amer. A*, vol. 24, no. 9, pp. 2737–2747, 2007.

[44] A. Pepe and R. Lanari, "On the extension of the minimum cost flow algorithm for phase unwrapping of multitemporal differential SAR interferograms," *IEEE Trans. Geosci. Remote Sens.*, vol. 44, no. 9, pp. 2374–2383, Sep. 2006.

[45] A. B. Giles, R. A. Massom, and R. C. Warner, "A method for sub-pixel scale feature-tracking using radarsat images applied to the Mertz Glacier Tongue, East Antarctica," *Remote Sens. Environ.*, vol. 113, no. 8, pp. 1691–1699, 2009.

[46] N. Riveros, L. Euillades, P. Euillades, S. Moreiras, and S. Balbarani, "Offset tracking procedure applied to high resolution SAR data on Viedma Glacier, Patagonian Andes, Argentina," *Adv. Geosci.*, vol. 35, pp. 7–13, 2013.

[47] A. Schubert, M. Jehle, D. Small, and E. Meier, "Influence of atmospheric path delay on the absolute geolocation accuracy of TerraSAR-X high-resolution products," *IEEE Trans. Geosci. Remote Sens.*, vol. 48, no. 2, pp. 751–758, Feb. 2010.

[48] X. Shi, L. Zhang, T. Balz, and M. Liao, "Landslide deformation monitoring using point-like target offset tracking with multi-mode high-resolution TerraSAR-X data," *ISPRS J. Photogrammetry Remote Sens.*, vol. 105, pp. 128–140, 2015.

Yu Chen received the B.S. degree in geographic information science and the master's degree in photogrammetry and remote sensing from the China University of Mining and Technology (CUMT), Xuzhou, China, in 2012, and the Ph.D. degree in earth and planetary science from the Federal University in Toulouse, Toulouse, France, in 2017.

She was an Assistant Researcher with the Géoscience Environment Toulouse Laboratory, French National Center for Scientific Research, in 2013. She is currently an Associate Professor with CUMT, Xuzhou. Her research interest is SAR interferometry, with particular emphasis on its application for geophysical studies.

Yunxiao Tong received the B.E. degree in surveying and mapping engineering from the Taiyuan University of Technology, Taiyuan, China, in 2017, and the M.E. degree in photogrammetry and remote sensing from the China University of Mining and Technology, Xuzhou, China, in 2020.

His research interest is synthetic aperture radar interferometry.

Kun Tan (Senior Member, IEEE) received the B.S. degree in information and computer science from Hunan Normal University, Hunan, China, in 2004, and the Ph.D. degree in photogrammetric and remote sensing from China University of Mining and Technology, Xuzhou, China, in 2010. From September 2008 to September 2009, he was a Joint Ph.D. candidate in remote sensing with Columbia University, New York, NY, USA.

From 2010 to 2018, he was with the Department of Surveying, Mapping, and Geoinformation, China University of Mining and Technology, Xuzhou, China. He is currently a Professor with East China Normal University, Shanghai, China. His research interests include hyperspectral image classification and detection, spectral unmixing, quantitative inversion of land surface parameters, and urban remote sensing.